

TRANSIENT SLOT COATING

Oldrich Joel Romero

Department of Mechanical Engineering, Pontifícia Universidade Católica do Rio de Janeiro
Rua Marquês de São Vicente 225, Gávea, CEP 22453-900, Rio de Janeiro, RJ, Brazil
oldrichjoel@yahoo.com.br

Márcio S Carvalho

Department of Mechanical Engineering, Pontifícia Universidade Católica do Rio de Janeiro
Rua Marquês de São Vicente 225, Gávea, CEP 22453-900, Rio de Janeiro, RJ, Brazil
msc@mec.puc-rio.br

Abstract. *In this work, the two-dimensional, transient flow that occurs during the deposition of a Newtonian liquid onto a substrate with a slot die is examined. The effect of an imposed persistent periodic (sinusoidal) perturbation of the liquid flow rate in the coated layer thickness variation is explored at different downstream lip length and coating gap (uniform, overbite and underbite) configurations. Small amplitude disturbances ($\sim 10\%$ and $\sim 1\%$) of the steady-state value are considered. The numerical solutions are obtained solving the governing Navier-Stokes equations, together with elliptic mesh generation technique of (Christodoulou and Scriven, 1992) and (de Santos, 1991) with appropriate boundary and initial conditions, by the Galerkin / finite element method. The temporal discretization is done by a predictor-corrector algorithm. The predictor step consists of a forward Euler method and the corrector step consist of a first-order fully-implicit Euler method. The resulting set of non-linear algebraic equations for the finite element basis functions' coefficients at each time step is solved by Newton's method. The results show how the process configuration may be optimize in order to minimize the effect of flow rate variation in the coated thickness.*

keywords: *slot coating, transient, free surface, galerkin*

1. Introduction

Flows with free surfaces and free boundaries arise in many industrial and biological applications. Examples are coating, polymer processing, ink-jet printing, spraying, deformation of blood cells, blood flow in arteries and capillaries, and flow in the deep pulmonary alveoli.

Many of these flows are time dependent, their dynamics are controlled by the viscosity, elasticity and capillarity of liquid. Modeling such flows requires computational methods which can describe and predict the flow field behaviour, while simultaneously capturing accurately the shape of free surfaces.

An enormous range of manufactured products involves layers deposited as a liquid and then solidified on a solid surface. Frequently, the coating stage of a manufacturing process is significant in cost, time involved and the level of technology required for the production. To be competitive in the marketplace, all aspect of the manufacturing must be efficient and maintain an acceptable level of quality control. Coating a substrate with a liquid is a question of practical interest together with a classical field of interfacial hydrodynamics. Products requiring precise control of coating thickness and avoidance of defects usually are coated with a pre-metering coating technique: the thickness of the coated liquid layer is set by the flow rate fed to the coating die and the speed of the moving substrate, and is independent of other process variables. Slot coating belongs to this class of coating methods. Thus pre-metered methods are ideal for high precision coating. However, the nature of the flow in the coating bead and the uniformity of the liquid layer it delivers can be affected by the substrate speed, liquid properties, configuration of the die lips and cross-web uniformity of the contact lines position.

Slot coating is commonly used in the manufacturing of adhesive and magnetic tapes, specialty papers, imaging films, and many other products. In this process, the coating liquid is pumped to a coating die in which an elongated chamber distributes it across the width of a narrow slot through which the flow rate per unit width at the slot exit is made uniform. Exiting the slot, the liquid fills (wholly or partially) the precise narrow channel (coating gap H_0 in the figure) between the adjacent die lips and the substrate translating rapidly past them. The liquid in the gap, bounded upstream and downstream by gas-liquid interfaces, or menisci, forms the coating bead.

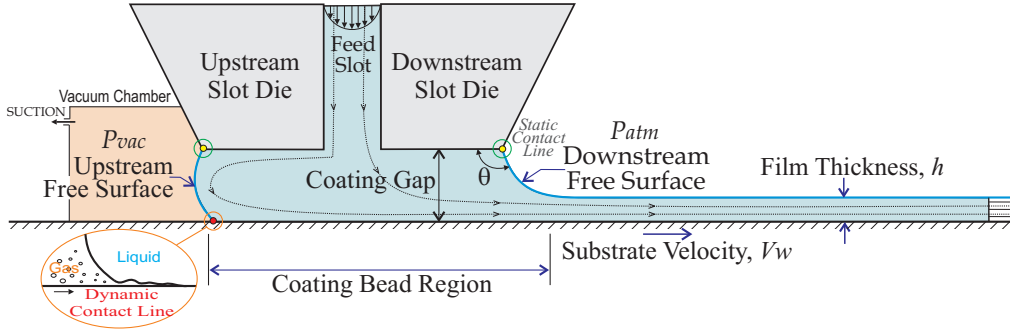


Figure 1: Side profile of the single layer slot coating. It includes many of the features that contribute to the technological complexity of the process.

Figure (1) shows a typical configuration of a die applicator and substrate. (Beguin, 1954) discovered that when layers thinner than about one-half the slot gap are to be coated (or in order to sustain the coating bead at higher substrate speeds), the forces on the coating bead go out of balance and that way to re-balance them is to apply a lower-than-ambient pressure in the upstream meniscus or “vacuum” (P_{vac} in the figure)), creating a Poiseuille flow that opposes the Couette flow driven by the web. This method has proven ineffective as a means of stabilization when the liquids are very viscous, i.e., thousands of centipoise. If not, instabilities which manifest themselves in a down-web (ribbing) or cross-web (rivulets) variations.

Physical dynamics is required to understand coating flows. The forces important in slot coating are viscous force, capillary force, pressure differences (or pressure gradients) forces, and in some cases inertial and elastic forces. Coating beads themselves are only possible when that forces are balanced.

In a problem with free surface, the physical domain is unknown a priori. Mesh equations must be added to the conservation equations to locate the free boundaries and map the unknown physical domain into a convenient reference one. Elliptic mesh generation method to solve 2-D free surface problem and domain deformation method to solve both 2-D and 3-D free surface problem for both structured and unstructured mesh. By these two methods, the unknown domain is solved simultaneously with the other variables.

In this work, the effect of the flow rate oscillation in the film thickness variation on slot coating process is currently being studied. In early works the effect of gravitational force was found to be usually of secondary importance and therefore not considered here. The mathematical modeling of the transient slot coating flow involves solving a initial boundary value problem in which the location of the free surface is a part of the solution of the problem. The unknown flow domain (physical) is mapped into a fixed domain (computational). The system of equations, with appropriate boundary conditions, for a two-dimensional viscous liquid flow is solved in coupled form by the Galerkin / finite element methods, where the temporal discretization is done by a predictor-corrector algorithm. The set of non-linear algebraic equations for the finite element basis functions is solved by Newton’s method.

This paper is organized as follow: First, the physical problem and mathematical formulation is presented. Second, a solution method is described which includes details of the free surface formulation, space and time discretization, and linearization. Finally the results and comments are presented.

2. Mathematical Formulation

The two-dimensional transient free surface flow depicted in Fig. (1) is defined by the governing Navier-Stokes and the continuity equations for a constant-property Newtonian liquid

$$\rho \left(\frac{\partial \mathbf{v}}{\partial t} + \mathbf{v} \cdot \nabla \mathbf{v} \right) - \nabla \cdot \mathbf{T} = 0, \quad (1)$$

$$\nabla \cdot \mathbf{v} = 0, \quad (2)$$

where \mathbf{v} is the liquid velocity, ρ is the liquid density, ∇ is the standard gradient operator, and t is the time. $\mathbf{T} = -p\mathbf{I} + \mu[\nabla \mathbf{v} + (\nabla \mathbf{v})^T]$ is the total stress tensor, the superscript T denotes transpose, p is the pressure, and μ is the Newtonian liquid viscosity. Body forces (i.e. gravity effects) are neglected.

The geometries where the governing equations are solved is sketched in Fig. (2). Four slot coating configurations with different downstream lip length and upstream coating gap are explored.

Appropriate boundary and initial conditions are necessary to uniquely solve this system of equations.

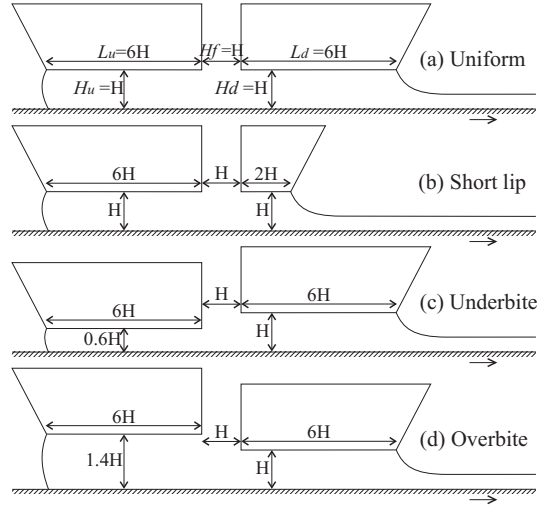


Figure 2: The four geometries used in this work in units of domain dimensions of the fixed downstream slot gap $H_d = 100 \mu\text{m}$. The upstream lip length L_u and feed slot H_f were also kept constant.

2.1. Boundary and initial conditions

The boundaries of the flow domain are labeled in Fig. (3), and the correspondent boundary conditions are:

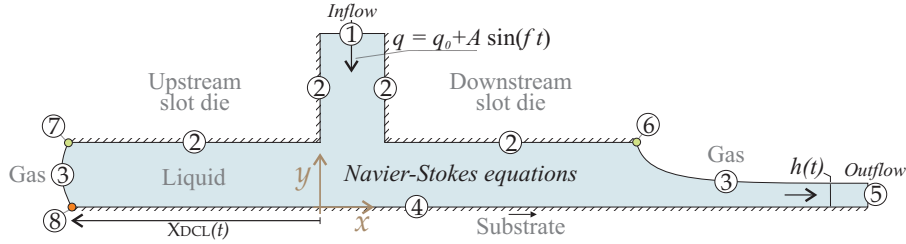


Figure 3: Labels for the boundary conditions in a slot coating process. The location of the two-dimensional cartesian coordinates is also shown.

(1)– At the two inflow planes, that is, at the die feeding slot, fully developed parallel rectilinear flow is assumed, where a Couette-Poiseuille velocity profile is prescribed in function of the base flow rate q_0 .

$$u = 0, \quad v = -\frac{6q_0}{H_f} \left[\left(\frac{x}{H_f} \right) - \left(\frac{x}{H_f} \right)^2 \right], \quad (3)$$

H_f if the feed slot considerer to be as $H_f = H_d = 100 \mu\text{m}$.

(2)– The no-slip and no-penetration conditions applies at the die walls.

$$u = 0, \quad v = 0. \quad (4)$$

(3)– At the free surfaces, the traction in the liquid balances the capillary pressure and there is no mass flow rate across the gas-liquid interface. The dynamic condition on the free surface are based on the continuity of the tangential stress (no traction) and discontinuity of normal stress caused by the surface tension. Implicitly is assumed that the flow activity outside the free surface is negligible with the atmospheric pressure taken as zero

$$\mathbf{n}_{fs} \cdot \mathbf{T} = \frac{1}{Ca} \frac{dt_{fs}}{ds} - \mathbf{n}_{fs} p_0, \quad (5)$$

$$\mathbf{n}_{fs} \cdot \left(\mathbf{v} - \frac{d\mathbf{x}}{dt} \right) = 0, \quad (6)$$

where $Ca \equiv \mu V_w / \sigma$ is the capillary number, dt_{fs}/ds represents the curvature of the meniscus, \mathbf{t}_{fs} and \mathbf{n}_{fs} are the local unit tangent and unit normal to the free surface, and p_0 is the pressure on the gas side. At the

downstream free surface, the gas pressure is usually atmospheric, that is $p_0 = P_{atm}$, and at the upstream free surface vacuum is applied in order to stabilize the coating bead, that is $p_0 = P_{vac}$. The evolution of the free surface is dictated by the kinematic condition Eq. (6).

(4)– In the moving substrate, the no-slip and no-penetration conditions are applied

$$u = V_w, \quad v = 0, \quad (7)$$

V_w is the substrate velocity.

(5)– At the outflow plane, fully developed flow is considered

$$\mathbf{n} \cdot \nabla \mathbf{v} = 0, \quad (8)$$

$\mathbf{n} \cdot \nabla$ is here the directional derivative parallel to the substrate.

(6)– The downstream static contact line, \mathbf{x}_d , is pinned to the sharp edge of the die

$$\mathbf{x}_d = (x_d, y_d). \quad (9)$$

(7)– The upstream static contact line is free to slide along the upstream die face H_u with a specified upstream static contact angle $\theta_u = 100^\circ$. The mathematical conditions are

$$y_u = H_u, \quad \mathbf{n}_w \cdot \mathbf{n}_{fs} = \cos(\theta_u), \quad (10)$$

\mathbf{n}_w is the unit vector normal to the wall.

(8)– At the web surface the liquid translates with the web except near the locations where the liquid first appears to contact the web. This sub-microscopic region is called the dynamic contact line, where evidences points a very thin film of air being entrained when the coating speed is high and to that air film breaking down and dissolving within around $100 \mu\text{m}$ of the dynamic contact line. In this short region the Navier slip condition was used instead of the no-slip condition and a dynamic contact angle $\theta_{dyn} = 110^\circ$ was specified.

$$\frac{1}{\beta} \mathbf{t}_w \cdot (\mathbf{v} - V_w \mathbf{i}) = \mathbf{t}_w \cdot (\mathbf{n}_w \cdot \mathbf{T}_1), \quad \mathbf{n}_w \cdot \mathbf{n}_{fs} = \cos(\theta_{dyn}), \quad (11)$$

where β is the slip coefficient, \mathbf{t}_w is the unit vector tangent to the wall. Without the slip condition there is a non-integrable singularity in shear stress. For a better description of the flow in this region, a contact angle as a function of a capillary number would be more appropriate or, as is mentioned in the work of (Weinstein and Ruschak, 2004), a new model could be used where the interfaces are considered to be thin fluid phases with equations of state relating in the simplest case, surface pressure to surface mass density.

Finally, an initial condition is needed. In this work, the fluid is assumed to be at rest initially, so the following condition holds

$$\mathbf{v}(x, y, t = 0) = 0. \quad (12)$$

The imposed perturbation liquid flow rate q is a linear combination of the base liquid flow rate q_0 and the disturbance sinusoidal in time mode $\Delta q = A \sin(f t)$

$$q = q_0 + A \sin(f t), \quad (13)$$

where A is the amplitude and f is the frequency of the imposed disturbance, and t is the time respectively. The ongoing disturbance in the liquid flow rate leads to an transient response.

2.2. Dimensionless parameters

The dimensionless parameters that governs the problem are: (i) Capillary number $Ca \equiv \mu V_w / \sigma$, which measures the ratio of viscous stress to pressure generated by surface tension in curved meniscus. Increasing the capillary number (which correspond to increase the production speed or the coating viscosity) usually shrinks the ranges of speed — that yield acceptably smooths films, μ is the viscosity of the liquid, V_w is the velocity of the flat wall or substrate, and σ the liquid surface tension. (ii) Reynolds number $Re \equiv \rho V_w / \mu$, ρ is the density of the liquid. (iii) Dimensionless vacuum pressure $Vac \equiv P_{vac} H_u / \sigma$. (iv) Gap-to-thickness ratio $g \equiv H_d / h_0$, h_0 is the base wet coating thickness deposited onto the substrate.

3. Solution method

3.1. Elliptic mesh generation

Because of the free surfaces, the flow domain is unknown *a priori*. The set of differential equations and boundary conditions posed in the unknown physical domain (x, y) has to be transformed to an equivalent set defined in a known reference domain fixed in time (ξ, η) (varying in the range $-1 \leq \xi \leq 1$ and $-1 \leq \eta \leq 1$), wherein a simple mesh tessellation is effected. This can be done with a mapping $\mathbf{x} = \mathbf{x}(\xi)$ that connects the two domains, as is shown in (Romero *et al.*, 1994 and Romero *et al.*,).

The mesh generation scheme must efficiently track the interface, maintain accuracy, smoothness, less danger of singularity and automatic local control of mesh properties throughout the entire domain. This is achieved using an elliptic mesh generation technique, described in detail (de Santos, 1991 and Benjamin, 1991). The inverse of the mapping is governed by a pair of elliptic differential equations

$$\nabla \cdot (\mathbf{D} \cdot \nabla \xi) = 0, \quad (14)$$

where $\nabla \equiv \partial/\partial \mathbf{x}$ denotes differentiation in physical space, and \mathbf{D} is the diffusivity-like adjustable tensor that allow for local grid refinement on the interior of the physical domain.

The governing and mesh generation equations written in the physical domain has to be rewritten in the reference domain. This procedure adds complexity.

Boundary conditions are needed before the second-order partial differential equation, Eq. (14), can be solved. The solid walls and synthetic inlet and outlet boundary planes were specified as functions of the coordinates and along them stretching functions were used to distribute the termini of the coordinate curves selected to serve as element sides. The free boundary – the gas-liquid interface or meniscus – is implicitly located by imposing the kinematic condition, Eq. (6).

In transient problems the frame of reference lies across the space-time domain for which the physical grid points are constantly updated in time, we must transform the time derivative at fixed Eulerian locations in space to time derivatives of any time-dependent quantity $\partial\Phi/\partial t$ at fixed iso-parametric coordinates, denoted by $\overset{\circ}{\Phi}$. The following transformation is employed

$$\frac{\partial \Phi}{\partial t} = \overset{\circ}{\Phi} - \overset{\circ}{\mathbf{x}} \cdot \nabla \Phi, \quad (15)$$

where, $\overset{\circ}{\mathbf{x}}$ is the mesh velocity (Christodoulou and Scriven, 1992). The time t is independent of either the original or he mapped coordinate system.

With relation from Eq. (15), the momentum equation becomes

$$\rho \left(\overset{\circ}{\mathbf{v}} + (\mathbf{v} - \overset{\circ}{\mathbf{x}}) \cdot \nabla \mathbf{v} \right) - \nabla \cdot \mathbf{T} = 0, \quad (16)$$

3.2. Reduction to ordinary algebraic equations by Galerkin finite element method with basis functions

The two-dimensional transient simulation were carried out using our in-house finite element analysis code, with the primitive variable (velocity-pressure) formulation and fully coupled solution methods -the position of the interface and the flow solution are computed simultaneously-

In the Galerkin's method, the governing partial differential equations, Eqs. (1), (2) and (14), are transformed into a discretized system of time-dependent ordinary differential equations multiplying by appropriate basis functions, integrating over the entire computational domain, and applying the divergence theorem to yield the weighted residual form.

$$R_i^m \equiv \int_{\bar{\Omega}} \left\{ \rho [\overset{\circ}{\mathbf{v}} + (\mathbf{v} - \overset{\circ}{\mathbf{x}}) \cdot \nabla \mathbf{v}] \psi_i^m + \nabla \psi_i^m \cdot \mathbf{T} \right\} J d\bar{\Omega} - \int_{\bar{\Gamma}} \psi_i^m (\mathbf{n} \cdot \mathbf{T}) \frac{d\bar{\Gamma}}{d\bar{\Gamma}} d\bar{\Gamma} = 0; \quad (17)$$

$$R_i^c \equiv \int_{\bar{\Omega}} (\nabla \cdot \mathbf{v}) \psi_i^c J d\bar{\Omega} = 0; \quad (18)$$

$$R_i^x \equiv - \int_{\bar{\Omega}} \nabla \psi_i^x \cdot \mathbf{D} \cdot \nabla \xi J d\bar{\Omega} + \int_{\bar{\Gamma}} \psi_i^x (\mathbf{n} \cdot \mathbf{D} \cdot \nabla \xi) \frac{d\bar{\Gamma}}{d\bar{\Gamma}} d\bar{\Gamma} = 0; \quad (19)$$

$$R_i^k \equiv \int_{\bar{\Gamma}} \mathbf{n} \cdot (\mathbf{v} - \overset{\circ}{\mathbf{x}}) \psi_i^k \frac{d\bar{\Gamma}}{d\bar{\Gamma}} d\bar{\Gamma} = 0; \quad (20)$$

Superscripts \mathbf{m} , c , \mathbf{x} , and k denotes momentum, continuity, mesh, and kinematic residuals; \mathbf{n} is the outward unit normal vector of the boundary Γ ; and $J = d\Omega/d\bar{\Omega}$ is the determinant of the mapping deformation gradient. This system is solved simultaneously to calculate the velocities, pressure and grid location of each node. The Galerkin weighted residuals are evaluated by nine-point Gaussian quadrature with three points in each computational direction.

Each independent variable is approximated with a linear combination of a finite number of known basis functions

$$\mathbf{v} = \sum_j^M \tilde{\mathbf{v}}_j(t) \varphi_j^{\mathbf{v}}(\xi, \eta), \quad p = \sum_j^N \tilde{p}_j(t) \varphi_j^p(\xi, \eta), \quad \mathbf{x} = \sum_j^M \tilde{\mathbf{x}}_j(t) \varphi_j^{\mathbf{x}}(\xi, \eta). \quad (21)$$

Here, $\tilde{\mathbf{v}}_j(t)$, $\tilde{p}_j(t)$, $\tilde{\mathbf{x}}_j(t)$, are the basis functions coefficients, and represents the unknowns of the discretized problem. The matrix vector of basis functions of the dependent variables is

$$\mathbf{u} \equiv [\tilde{\mathbf{v}}_j(t), \tilde{p}_j(t), \tilde{\mathbf{x}}_j(t)]^T. \quad (22)$$

An efficient mixed formulation of continuous basis functions are used to expand the independent variables. Lagrangian biquadratic polynomials for velocity $\varphi^{\mathbf{v}}(\xi, \eta)$ and position $\varphi^{\mathbf{x}}(\xi, \eta)$, and linear discontinuous for pressure $\varphi^p(\xi, \eta)$ were used. The polynomial basis functions constructed on a standard square domain (ξ, η) (where $-1 \leq \xi \leq 1$ and $-1 \leq \eta \leq 1$) was mapped into each of the deformed quadrilateral elements in the flow domain by the time-dependent isoparametric mapping.

In the weak (Galerkin) form equations, the weighting or test functions are the same of the basis functions, i.e. $\psi^{\mathbf{m}} = \varphi^{\mathbf{v}}$, $\psi^c = \varphi^p$ and $\psi^{\mathbf{x}} = \varphi^{\mathbf{x}}$.

By means of the Galerkin/FEM combined with the elliptic mesh generation system, equations are reduced into a set of ordinary differential and algebraic equations for the coefficient of the basis functions of the form

$$\mathbf{R}(\mathbf{u}, \dot{\mathbf{u}}, \mathbf{q}) = 0, \quad (23)$$

where \mathbf{R} is the set of weighted residual equations, \mathbf{u} is a matrix vector of basis functions (unknowns) of the dependent variables given by Eq. (22), $\dot{\mathbf{u}}$ is their time derivatives, and \mathbf{q} the vector of input (physical and discretization) parameters. The governing equations are solved in a couple manner, simultaneously everywhere.

3.3. Time integration

The aforementioned Galerkin weighted residuals form a set of nonlinear ordinary differential equations and algebraic equations in time. The temporal discretization of this set of equations is done by a predictor corrector algorithm. The predictor step consists of a forward Euler method and the corrector step consists of a first-order fully implicit Euler method, which is unconditionally stable in the sense that the time step is not restricted by any CFL-condition. The approximate form of the velocity time-derivatives in the momentum conservation equation, Eq. (16), using backward finite difference is

$$\overset{\circ}{\mathbf{v}} \equiv \frac{\mathbf{v}_{n+1} - \mathbf{v}_n}{t_{n+1} - t_n} = f(\mathbf{v}_{n+1}, t_{n+1}), \quad (24)$$

where the index $n + 1$ and n indicates current and previous time instant respectively. The difference $t_{n+1} - t_n$ defines the current time step Δt_{n+1} . A similar expression is used for the mesh velocity $\overset{\circ}{\mathbf{x}}$.

3.4. Evaluation of the basis functions coefficients

The resulting set of nonlinear algebraic equations (in $n + 1$) is solved simultaneously by the Newton's method with an initial estimate resulting from an explicit Euler step from the solution at the previous time. At each time step solve

$$\left(\frac{1}{\Delta t} \mathbf{M} + \mathbf{J} \right) \delta \mathbf{u}^{(k+1)} = -\mathbf{R}(\mathbf{u}^{(k+1)}, \mathbf{u}^k), \quad (25)$$

$$\mathbf{u}^{(k+1)} = \mathbf{u}^k + \delta \mathbf{u}^{(k+1)}, \quad (26)$$

Newton's method linearize the equation set and adds the solution of the resulting linear system to the current estimate in order to provide an updated estimate of the flow field. The iteration is repeated until convergence. Here $\mathbf{J} \equiv \partial \mathbf{R} / \partial \mathbf{u}$ is the Jacobian matrix which measure the sensitivity of the residuals to changes in the nodal unknowns and $\mathbf{M} \equiv \partial \mathbf{R} / \partial \dot{\mathbf{u}}$ is the mass matrix and measure the sensitivity of the residuals to changes in the time derivatives of the nodal unknowns (liquid accelerations, velocities and nodal points). The integrals arising

in the residuals and the Jacobian matrices used in Newton’s method are evaluated numerically using Gaussian quadrature (Strang and Fix, 1973).

Because the finite element basis functions used are different from zero only over a very small portion of the domain, the Jacobian matrix is sparse and was stored in compressed sparse formats. In each Newton iteration, the linearized equation system was factorized into unit lower L and unit upper U triangular matrix by a Gauss-elimination direct frontal solver (Hood, 1976 and Hood, 1977), as described by (Almeida, 1996).

In order that the Newton process converged within 6 to 8 iterations at each successive new set of operating conditions, the initial estimates were generated by a pseudo-arc-length continuation method as described by (Keller, 1977 and Bolstad and Keller, 1985). The tolerance on the L_2 -norm of the residual vector and on the last Newton update of each declared solution was set to 10^{-6} . However, close to turning points where the Jacobian matrix becomes singular, convergence becomes difficult or impossible. Turning points are where a solution branch turns back on itself. Other singular points are the bifurcation points and Hopf points.

3.5. Mesh selection and computer implementation

A mesh convergence analysis was done by comparing the downstream free surface configuration at capillary number $Ca = 0.2$, Reynolds number $Re = 1.33$, dimensionless vacuum pressure $Vac = 12$, and gap-to-thickness ratio $H_d/t = 5$.

The insensitivity of computed solutions to further mesh refinement has been demonstrated by systematically increasing the level of refinement near the interface in the coating bead region for the uniform coating configuration, Fig. 2-a. Three different meshes was tested refined until the results changed by less than 1 %. In this work the mesh selected contains 328 elements with 1,421 nodes.

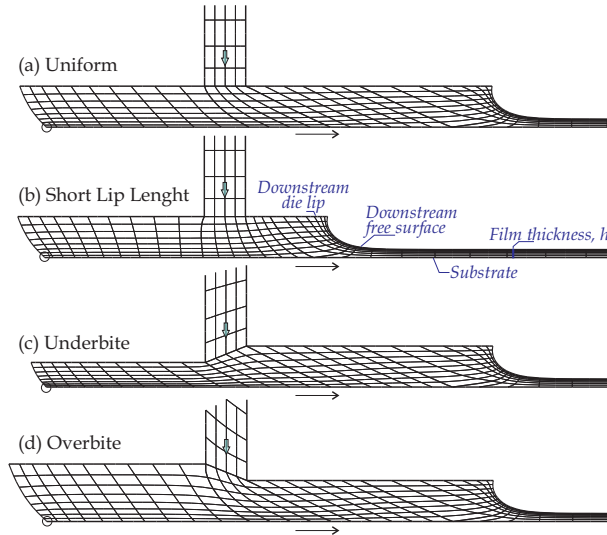


Figure 4: Close-up view of the tessellated domain for each slot coater configuration.

For each geometry explored (uniform, short lip length, underbite and overbite) the typical meshes used are showed in Fig. 4. The total number of basis functions coefficients is 6,668. The resulting algorithm have been programmed in FORTRAN and run on a single 2.4 GHz Intel(R) Pentium(R) IV processor. A typical transient simulation of the slot coater requires roughly 50 minutes for 100 time steps, each Newton’s iteration takes around 30 seconds.

4. Results and discussion

Limitations of this computational experiments include the inability to scan the enormous range parameter space encompassed by the single slot coater process. The parameter space is a function of several variables including Reynolds number, Stokes number, capillary number, gap-to-thickness ratio, vacuum level, die shape, and more. Hopefully, the representative studies presented here will raise awareness for the need of more research in the field of one coating analysis.

Solutions were computed at different capillary and Reynolds numbers, and several liquid flow rate, constant gap-to-thickness ratio H_0/t and vacuum level Vac .

Figure (5) displays contours of the transient streamfunction at three time instant $t_1 = 22\Delta t$, $t_2 = 38\Delta t$ and

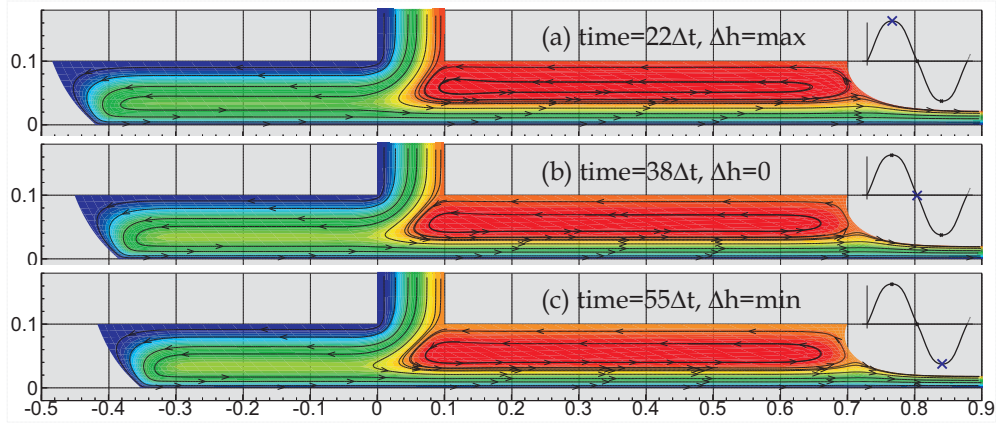


Figure 5: Three time instant showing the flow field variation with time in a parallel coating gap corresponding to the red curve of Fig. (9). The flow rate oscillates with amplitude $A = 10\%$ and frequency $f = 500$ Hz.

$t_3 = 55\Delta t$ which correspond to a maximum ($h_1 = h_0 + \Delta h_0$), middle ($h_2 = h_0$) and minimum ($h_3 = h_0 - \Delta h_0$) film thickness respectively. Some fraction of the liquid moves into the upstream bead, whereas a remainder flows into the downstream bead. The net flow into the upstream portion of the bead equals zero, the upstream meniscus bounds the liquid and the flow turns 180° . The upstream meniscus meets the web at the dynamic contact angle $\theta_{dyn} = 120^\circ$ and intersects the upstream slot lip at the static contact angle $\theta_{sca} = 70^\circ$. Under the downstream lip, where viscous and pressure forces balance each other, the flow is largely rectilinear until the liquid squeezes under the downstream meniscus and the streamlines become curved and inertia plays a greater role. The liquid accelerates until it reaches the web speed. Over roughly three gaps downweb from the downstream lip edge, the liquid relaxes to a thin film that is essentially plug flow, viscous and inertial forces diminish. The free surface curvature is highest close to the downstream lip edge, where the contact line is pinned, and drops rapidly away and the free surface levels out. The concavity of the meniscus (from the gas side) requires that the pressure be sub-ambient.

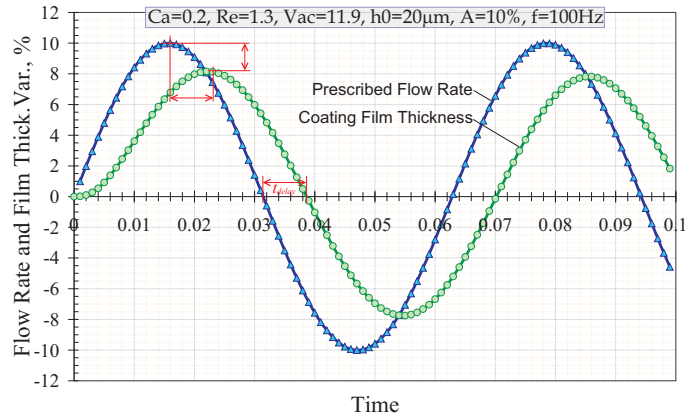


Figure 6: Transient film thickness variation with amplitude A of the sinusoidal perturbation of the input flow rate ($q = q_0 + A \sin(ft)$) in a uniform slot configuration.

The curvature of the downstream meniscus increase and the dynamic contact line moves towards the feed slot diminishing the coating bead length and because the disturbance introduced into the prescribed flow rate is a sinusoidal function, the coating film thickness and the dynamic contact line respond in a similar form. Fig. (6) presents the transient flow rate prescribed at the inflow plane with amplitude $A = 10\%$ and frequency $f = 100$ Hz, and the transient coating film thickness measured at the outflow plane (see Fig. (3)). As observed, the perturbation takes a time until produce a response in the output film thickness, this is the delay time (t_{delay} in the figure) which is function of the operating parameters, liquid properties and perturbation.

The influence of the amplitude of the perturbation in the film thickness is explored in Figs. (7) and (8), shows that the higher the liquid flow rate, the higher the response to ongoing disturbances of the flow rate, and

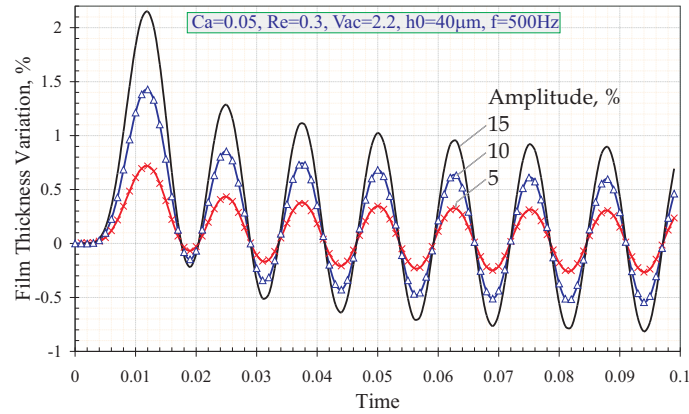


Figure 7: Transient film thickness variation with amplitude A of the sinusoidal perturbation of the input flow rate ($q = q_0 + A \sin(ft)$) in an uniform slot configuration.

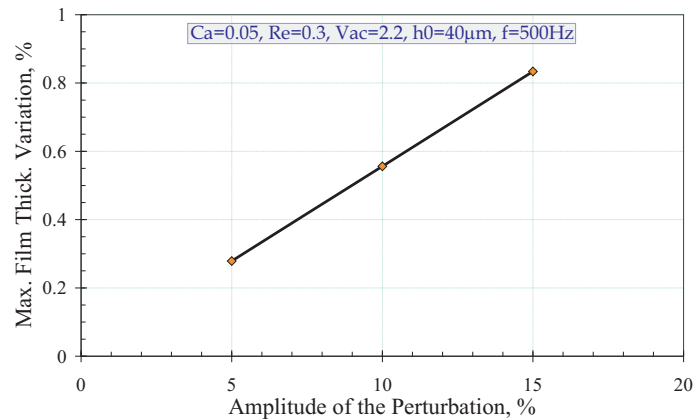


Figure 8: Variation of the final liquid layer thickness with the amplitude of the perturbation of the liquid flow rate in the uniform slot coating.

as is displayed in Fig. (8) this growth is linear. This result agrees very well with the obtained by (Gates, 1999) in his frequency response analysis of slot coating. The perturbations imposed by (Gates, 1999) had amplitude of 1% and frequencies ranging from 1 to 2000 Hz.

Figures (9) and (10) plots the transient coating film thickness variation at frequencies ranging from 100 Hz to 1000 Hz. The results shows that the higher the frequencies of the ongoing disturbances of the flow rate, the lower the film thickness variation. This results are in accordance with the results obtained by (Gates, 1999). Fig. (10) also shows higher the amplitude of the perturbation, the higher the variation of the film thickness.

The influence of the capillary number is plotted in Fig. (11), the coating film thickness varies in inverse proportion to the capillary number. Figure (12) shows how the film thickness change as the coating gap passes from the underbite to overbite configuration at constant capillary and Reynolds number. The underbite configuration is when the upstream gap is narrower than the downstream gap. The overbite is when the upstream gap is wider than the downstream gap.

5. References

- Almeida, V. F., 1996, “Gas-Liquid counterflow through constricted passages”, PhD thesis, University of Minnesota, USA.
- Beguín, 1954, US Patent 2681294.
- Benjamin, D. F., 1991, “Roll Coating Flows and Multiple Rolls Systems”, PhD thesis, University of Minnesota, USA.
- Bolstad, J. H. and Keller, H. B., 1985, A multigrid continuation method for elliptic problems whit folds, “SIAM

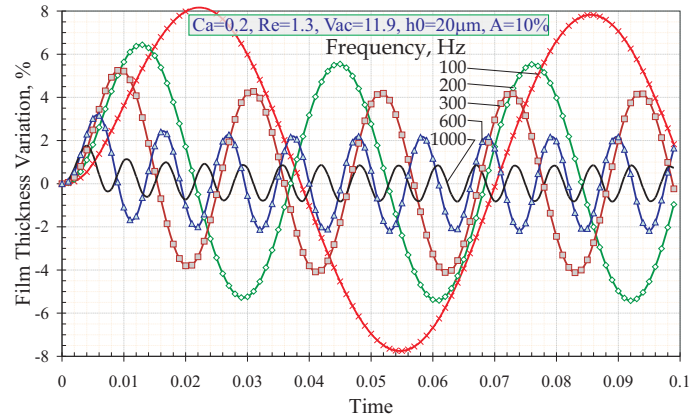


Figure 9: Transient film thickness variation with frequency f of the sinusoidal perturbation of the input flow rate ($q = q_0 + A \sin(ft)$) in an uniform slot configuration.

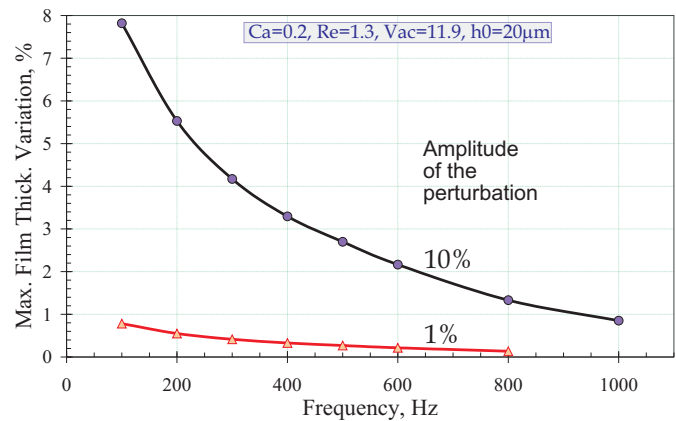


Figure 10: Variation of the final liquid layer thickness caused by 1% and 10% perturbation of the liquid flow rate in the uniform slot coating.

Journal of Science Stat. Comput.”, Vol. 7, pp. 1081–1104.

Christodoulou, K. N. and Scriven, L. E., 1992, Discretization of free surface flows and other moving boundary problems, “J. Comput. Phys.”, Vol. 99, pp. 39–55.

de Santos, J. M., 1991, “Two-phase Cocurrent Downflow Through Constricted Passages”, PhD thesis, University of Minnesota, USA.

Gates, I. D., 1999, “Slot Coating Flows: Feasibility, Quality”, PhD thesis, University of Minnesota, USA.

Hood, P., 1976, Frontal Solution Program for Unsymmetric Matrices, “Int. J. Numer. Meth. Eng.”, Vol. 10, pp. 379–399.

Hood, P., 1977, Correction, “Int. J. Numer. Meth. Eng.”, Vol. 11, pp. 1055.

Keller, H. B., 1977, “Numerical solution of bifurcations and nonlinear eigenvalue problems in Applications of Bifurcation Theory”, Academic Press, New York, USA.

Romero, O. J., Scriven, L. E., and Carvalho, M. S., Slot coating of mildly viscoelastic liquids, “Journal of Non-Newtonian Fluid Mechanics”, , No. doi 10.1016/j.jnnfm.2005.11.010.

Romero, O. J., Suszynsky, W. J., Scriven, L. E., and Carvalho, M. S., 1994, Low-flow Limit in Slot Coating of Dilute Solutions of High Molecular Weight Polymer, “Journal of Non-Newtonian Fluid Mechanics”, Vol. 118, pp. 137–156.

Strang, G. and Fix, G. J., 1973, “An Analysis of Finite Element Method”, Printice-Hall, USA.

Weinstein, S. J. and Ruschak, K. J., 2004, Coating Flows, “Annu. Rev. Fluid Mech.”, Vol. 36, pp. 29–53.

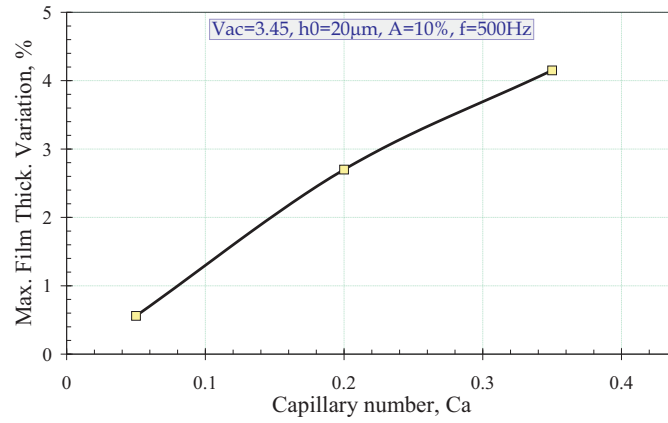


Figure 11: Influence of the capillary number (Ca) in the film thickness.

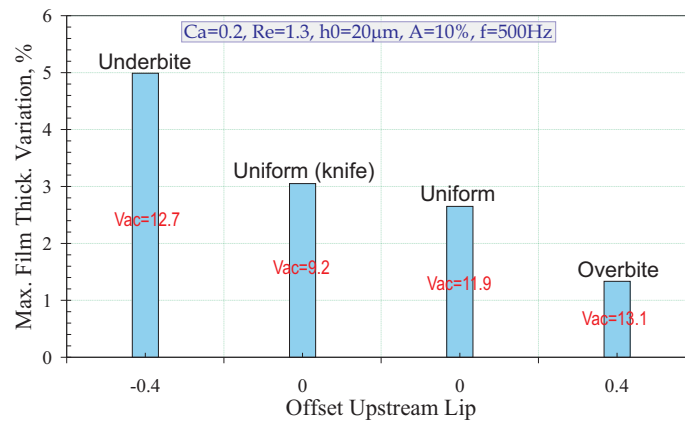


Figure 12: Maximal film thickness variation at different coating gap and lip length configurations.

6. Author rights

The authors are the only responsible for the printed material included in his papers.